

STPrivacy: Spatio-Temporal Tubelet Sparsification and Anonymization for Privacy-preserving Action Recognition

Ming Li¹ Jun Liu² Hehe Fan³ Jia-Wei Liu⁴ Jiahe Li³
Mike Zheng Shou⁴ [†] Jussi Keppo⁵

¹Institute of Data Science, National University of Singapore

²Singapore University of Technology and Design

³School of Computing, National University of Singapore

⁴Show Lab, National University of Singapore

⁵Business School, National University of Singapore

Abstract

Recently privacy-preserving action recognition (PPAR) has been becoming an appealing video understanding problem. Nevertheless, existing works focus on the frame-level (spatial) privacy preservation, ignoring the privacy leakage from a whole video and destroying the temporal continuity of actions. In this paper, we present a novel PPAR paradigm, i.e., performing privacy preservation from both spatial and temporal perspectives, and propose a STPrivacy framework. For the first time, our STPrivacy applies vision Transformers to PPAR and regards a video as a sequence of spatio-temporal tubelets, showing outstanding advantages over previous convolutional methods. Specifically, our STPrivacy adaptively treats privacy-containing tubelets in two different manners. The tubelets irrelevant to actions are directly abandoned, i.e., sparsification, and not published for subsequent tasks. In contrast, those highly involved in actions are anonymized, i.e., anonymization, to remove private information. These two transformation mechanisms are complementary and simultaneously optimized in our unified framework. Because there is no large-scale benchmarks, we annotate five privacy attributes for two of the most popular action recognition datasets, i.e., HMDB51 and UCF101, and conduct extensive experiments on them. Moreover, to verify the generalization ability of our STPrivacy, we further introduce a privacy-preserving facial expression recognition task and conduct experiments on a large-scale video facial attributes dataset, i.e., Celeb-VHQ. The thorough comparisons and visualization analysis demonstrate our significant superiority over existing works. The appendix contains more details and visualizations.

[†]Corresponding Author.

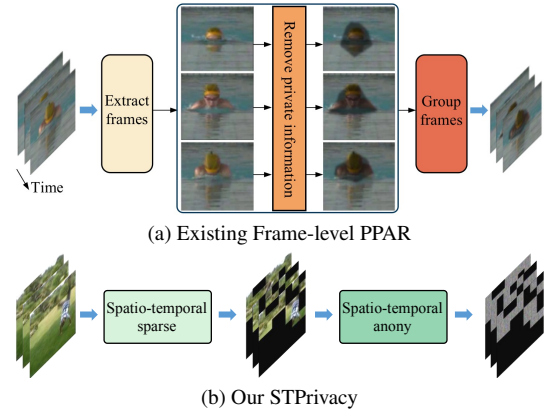


Figure 1. Comparison of existing PPAR methods with our STPrivacy. (a) Existing methods remove private information from each frame separately. They ignore the possibility of privacy leakage from a whole video, which, in practice, is more likely exploited by an intruder. Moreover, they do not consider dynamics of actions. (b) Our STPrivacy is proposed to protect privacy from spatio-temporal perspectives and emphasize the continuity of actions by performing adaptive tubelet sparsification (spars) and anonymization (anony). The black and colored areas represent the abandoned and anonymized remaining tubelets by our method, respectively.

1. Introduction

Action recognition is a fundamental video understanding problem [11, 13, 35, 37]. To facilitate the research under diverse scenarios, various datasets are collected, e.g., HMDB51 [20], UCF101 [31], ActivityNet [4], and FineGym [30]. Although the availability of these datasets indeed advances the development of relevant algorithms, it meanwhile brings a tricky problem. Namely, the collected videos usually contain personal information and have a potential threat to human privacy. Therefore, it is desirable to develop privacy-preserving action recognition (PPAR) methods that prevent privacy leakage from videos but maintain

action clues.

The PPAR problem has been investigated from various points of view, *e.g.*, reducing video resolution [3, 5, 6, 22, 29, 32], altering sensitive areas [27, 42], and learning-based anonymization [7, 39, 40]. As illustrated in Figure 1, they use the same paradigm that can be described as three basic steps, *i.e.*, extracting frames from a video, separately removing private information in each frame, and grouping processed frames together for recognition. On the one hand, these works only realize frame-level (spatial) privacy protection rather than video-level. However, preventing the privacy leakage from an entire video is much more practical and challenging. For example, to protect frame-level facial information against an intruder, an anonymization model only needs to erase parts of regions of a face so that solely identifying the face from each frame is unsuccessful. But it is still easily reachable for a deep neural network model to recognize the face from the entire video by aggregating clues from all frames, which is highly similar to the occluded object recognition from videos [15, 16, 38, 43]. This is due to the high information redundancy and complementing property of video data [12, 33]. On the other hand, anonymizing each frame separately will inevitably destroy the coherence of actions, degrading action recognition performance. Additionally, the only benchmark PA-HMDB [39] for evaluating current PPAR methods is pretty small and can not convincingly prove their capability.

To tackle these issues, we propose a novel PPAR paradigm and a framework STPrivacy that balances action recognition (utility) and video-level privacy recognition (budget) from both spatial and temporal perspectives. Our STPrivacy introduces vision Transformers (ViTs) [10] for PPAR and treats a video as a sequence of spatio-temporal tubelets. It applies two mechanisms to adaptively transform the tubelets, removing private information and meanwhile maintaining action clues. Specifically, our STPrivacy directly abandons the tubelets that contain privacy and do not affect action dynamics, *i.e.*, sparsification. As for those tubelets that contain both private and action information, our STPrivacy removes privacy from them in the representation space, *i.e.*, anonymization. These two mechanisms are performed simultaneously under the guidance of a minimax optimization objective. Additionally, to construct large-scale video-level PPAR benchmarks, we annotate five human privacy attributes for two of the most popular action recognition datasets, *i.e.*, HMDB51 [20] and UCF101 [31].

In summary, our main contributions are as follows:

- Our STPrivacy is the first work to perform the video-level PPAR research and introduces ViTs into this area, which exhibits advantages in achieving visually complete privacy removal and easily balancing the trade-off between the utility and budget tasks.
- We propose to employ the spatio-temporal sparsifica-

tion and anonymization to transform action-irrelevant and action-involved privacy tubelets, respectively.

- We construct two large-scale video-level PPAR benchmarks that will be released to the community.
- Our STPrivacy sets new state-of-the-art (SOTA) trade-offs between the utility and budget tasks on two benchmarks. The qualitative visualizations also show its effectiveness and superiority.
- The generalization ability of our framework is demonstrated on another task, *i.e.*, privacy-preserving facial expression recognition based on CelebVHQ [45].

2. Related works

2.1. Privacy-preserving action recognition

Previous works on PPAR can be grouped into three mainstreams according to their applied privacy-removing techniques, *i.e.*, simply downsampling [3, 5, 6, 22, 29, 32], offline obfuscation [27, 42], and learning-based anonymization [7, 39, 40]. Intuitively, resolution downsampling is an effective way to reduce privacy leakage. But the low resolution will also cause difficulties to action recognition [3, 5, 32]. Obfuscation methods first detect sensitive regions from video frames by using an off-the-shelf detector and then alter the regions in an offline manner. The performances of these methods heavily depend on the efficacy of pre-trained detectors. Moreover, the obfuscation techniques only change the data distribution of the detected regions, which brings severe data distribution gaps within a frame [27, 42]. Learning-based anonymization methods are much more promising for maintaining the utility performance [7, 39, 40]. However, they only focus on the frame-level privacy preservation by separately removing private information from each frame. In contrast, we propose to perform the video-level PPAR from both spatial and temporal perspectives, which is more in line with practical applications and moreover takes action coherence into consideration when transforming a raw video.

2.2. Vision Transformer

Self-attention [36] inspired Transformers are proven to have inborn properties of capturing long-distant correlations in various natural language processing problems [9, 44]. Initially, ViT [10] introduced Transformers into vision tasks by dividing an image into a series of rectangle patches and embedding tokens from them. To efficiently encode spatio-temporal representations for video understanding, ViViT [1] and Timesformer [2] investigated various self-attention factorization techniques. Recently, several works propose to perform efficient ViT inference by gradually pruning less informative tokens during computation [19, 25, 26]. Although abandoning tokens also occurs in our framework, ours differs from efficient ViTs (EViTs) on at least three as-

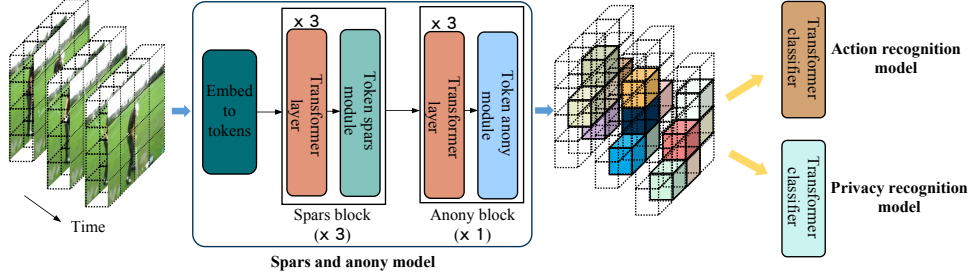


Figure 2. Overview of our STPrivacy. It consists of three models, *i.e.*, a spars and anony (SA) model, an action recognition (utility) model, and a privacy recognition (budget) model. The core of PPAR is to optimize the SA model with the objective of maintaining action clues and removing private information as much as possible when transforming an input raw video. In this way, the utility model can still perform very well on the transformed video, while the performance of the budget model degrades largely. The dashed cubes represent the input and output tubelets. The blank cubes denote the abandoned privacy-containing action-irrelevant tubelets, while the colored are the anonymized remaining action-relevant tubelets by our SA model.

pects. Firstly, our STPrivacy has a significantly different sparsification mechanism. In EViTs, the information from less informative tokens has actually been aggregated into the classification token before being pruned [19, 25, 26]. In other words, these tokens are implicitly involved in the final prediction. In our framework, however, the abandoned tokens have no chance of contributing to the subsequent utility or budget tasks, which means that our sparsification is more difficult. Secondly, the success of EViTs typically depends on the sophisticated distilled knowledge from the prediction logits and token embeddings of a vanilla ViT teacher [19, 25, 26], which is not needed in our STPrivacy. Finally, except the sparsification, our framework also incorporates a tubelet anonymization mechanism that is proven to considerably promote the performances. These differences tell that our work is much more challenging.

3. Spatio-temporal tubelet sparsification and anonymization

The illustration of our framework is shown in Figure 2. It contains a SA model, a utility model and a budget model. The SA model is derived from a vanilla ViT [10] that is also employed as the utility and budget models. No classification token is used here. In specific, the SA model consists of three stacked spars blocks followed by an anony block. The former aims to sparsify video tubelets and the latter is responsible for anonymizing remaining ones. They are performed simultaneously under the guidance of a min-max optimization objective. Each spars block comprises three Transformer layers, whose self-attention is only computed among remaining tokens, and a token spars module. The anony block has a similar structure except the anony module. Firstly, the tokens embedded from spatio-temporal tubelets pass through three spars blocks sequentially. Those tokens containing private information but no action clues are gradually abandoned by the spars modules. Then the remaining tokens are further anonymized by the anony block to remove privacy. Finally, the transformed output from

the SA model is fed into the utility and budget models for recognition.

3.1. Preliminaries

Given a training set $\mathcal{D} = \{(x_i, y_i, p_i)\}_{i=1}^N$, $x_i \in \mathbb{R}^{T \times H \times W \times 3}$ is a video, $y_i \in \{0, 1\}^C$ is its one-hot action label over C classes, and $p_i \in \{0, 1\}^P$ represents its multi-class binary privacy annotation over P classes. A sequence of tokens $e_i \in \mathbb{R}^{t \times s \times f}$ are embedded from x_i using a 3D convolution layer with the stride $\delta T \times \delta H \times \delta W$ followed by flattening spatial dimensions. Thus each token corresponds to a tubelet with the shape $\delta T \times \delta H \times \delta W \times 3$. We maintain a binary keeping decision matrix $\hat{\mathbf{I}}_i \in \{0, 1\}^{t \times s}$ whose elements are initialized as 1. A element value denotes whether the corresponding token is abandoned (0) or not (1) [26]. Note that the first two dimensions of e_i and $\hat{\mathbf{I}}_i$ are flattened when they pass through Transformer layers.

3.2. Tubelet sparsification

As mentioned, our token spars modules are devised to abandon privacy-containing tokens (tubelets) which have no effect on the utility task. In each module, we first aggregate spatial and spatio-temporal information into each token to collect multi-level features. In detail, a multi-layer perceptron (MLP) consisting of one linear layer followed by the GELU activation [14] is applied to change the embedding dimension of tokens e (the subscript is omitted for simplicity) from the preceding Transformer layer as new token features:

$$e^{\text{token}} = \text{MLP}_1(e) \in \mathbb{R}^{t \times s \times f/3}. \quad (1)$$

Projecting e by another MLP, the spatial features e^{spatio} are obtained based on the previous token keeping decision $\hat{\mathbf{I}}$:

$$e^{\text{spatio}} = \text{Expd}(\text{Avg}(\text{MLP}_2(e), \hat{\mathbf{I}})) \in \mathbb{R}^{t \times s \times f/3}, \quad (2)$$

where Avg and Expd represent sequentially averaging a 3D tensor and expanding by repeating it on the second dimension. In Avg, only the remaining tokens denoted by 1 in $\hat{\mathbf{I}}$ participate in the computation. In a similar way, we get the spatio-temporal features e^{spattem} :

$$e^{\text{spatem}} = \text{Expd}(\text{Avg}(\text{MLP}_3(e), \hat{\mathbf{I}})) \in \mathbb{R}^{t \times s \times f/3}, \quad (3)$$

where Avg and Expd are performed across the first two dimensions. These hierarchical features are combined together by concatenating on the last dimension:

$$e^{\text{hier}} = \text{Concat}(e^{\text{token}}, e^{\text{spatio}}, e^{\text{spatem}}). \quad (4)$$

Then, to predict keeping probabilities of tokens, an MLP consisting of three linear layers is employed to gradually reduce the embedding dimension of e^{hier} , followed by a Softmax operation:

$$z = \text{Softmax}(\text{MLP}_4(e^{\text{hier}})) \in \mathbb{R}^{t \times s \times 2}. \quad (5)$$

Finally, to make the sparsification differentiable, the Gumbel-Softmax technique [17, 19, 26] is applied:

$$\mathbf{I} = \text{GumbelSoftmax}_{[0]}(z) \in \{0, 1\}^{t \times s}. \quad (6)$$

The subscript of GumbelSoftmax means that we take the current keeping results from the last dimension. The previous token keeping decision $\hat{\mathbf{I}}$ is renewed by its Hadamard product with \mathbf{I} and fed into subsequent Transformer layers along with the tokens e .

Self-attention only for remaining tokens. During inference, it is feasible to maintain the specific (same) number of tokens for each input by performing argsort, *i.e.*, sorting the keeping probabilities $z_{[0]}$ of all tokens. The tokens with lower keeping scores are indeed abandoned and do not occur in following computations. Therefore, the self-attention can be directly computed only amongst the remaining tokens [19, 26]. During training, in contrast, the number of remaining tokens for each input probably differs. It is computationally unfriendly to indeed abandon the tokens denoted by 0 in $\hat{\mathbf{I}}$ from each input. With all tokens occurring, we compute the self-attention matrix $\tilde{\mathbf{P}}$ [36] as follows:

$$\mathbf{S} = \mathbf{Q}\mathbf{K}^T / \sqrt{f} \in \mathbb{R}^{ts \times ts}, \quad (7)$$

$$\mathbf{W}_{m,n} = \begin{cases} 1, & m = n, \\ \hat{\mathbf{I}}_n, & m \neq n. \end{cases} \quad 1 \leq m, n \leq ts, \quad (8)$$

$$\tilde{\mathbf{P}}_{mn} = \frac{\exp(\mathbf{S}_{mn})\mathbf{W}_{mn}}{\sum_{k=1}^{ts} \exp(\mathbf{S}_{mk})\mathbf{W}_{mk}}, \quad 1 \leq m, n \leq ts. \quad (9)$$

3.3. Tubelet anonymization

It is probable that many video tubelets not only contain private information but also play critical roles in representing an action. Therefore, directly abandoning these tubelets hinders the utility performance heavily. To tackle this issue, our token anony module is present to learn privacy-irrelevant action representations by itself. Referring to the literature [7, 39, 40], the transformed counterpart of a raw input video should also be a video. Thus, the final output of our SA model should contain a sequence of “tubelets”, as illustrated in Figure 3. To match the size of flattened tubelets,

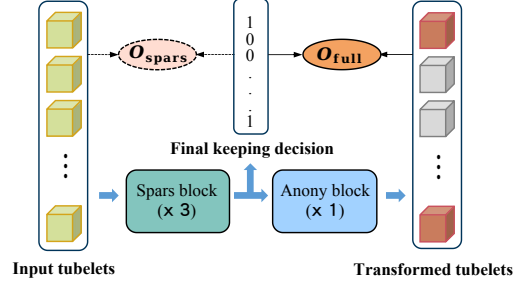


Figure 3. The output of our SA model for optimizing the separate sparsification only (O_{spars}) or both the sparsification and anonymization (O_{full}). The grey cubes are abandoned tubelets.

we employ an MLP to change the embedding dimension of the tokens e passed into the token anony module:

$$e^{\text{out}} = \text{MLP}_5(e) \in \mathbb{R}^{t \times s \times 3\delta T \delta H \delta W}. \quad (10)$$

As mentioned, in the inference mode of the SA model, e^{out} only contains the remaining tubelets by performing argsort. It is directly fed into the utility and budget models for recognition. In the training mode, e^{out} contains all tubelets. Thus, the final keeping decision $\hat{\mathbf{I}}$ together with the anonymized tubelets e^{out} , *i.e.*, O_{full} in Figure 3, should be passed into the utility and budget models for computing self-attention only amongst the remaining tokens.

3.4. Learning procedure and objectives

In general, the whole procedure of performing PPAR contains three stages, *i.e.*, framework initialization, minimax optimization of the SA model, and training target utility and budget models.

To control the number of remaining tokens from the SA model, we set the gradually decreasing keeping ratio α^k , $\alpha = 0.7$ for the k th spars block. Then the decision matrix $\hat{\mathbf{I}}^{(k)}$ of the k th spars block is supervised by an MSE loss:

$$\mathcal{L}_{\text{ratio}} = \frac{1}{3t} \sum_{k=1}^3 \sum_{m=1}^t \left(\frac{1}{s} \sum_{n=1}^s \hat{\mathbf{I}}^{(k)}(m, n) - \alpha^k \right)^2. \quad (11)$$

The objective for the utility model is a classification cross-entropy loss $\mathcal{L}_{\text{utility}}$ derived from its class prediction and the action label \mathbf{y} . As for the budget model, the objective is a multi-class binary cross-entropy loss $\mathcal{L}_{\text{budget}}$ derived using its prediction and the privacy annotation \mathbf{p} .

Framework initialization. To stabilize the minimax optimization, we first initialize our framework using raw videos as inputs. In the SA model, we add an auxiliary classification token for predicting an action and deriving a cross-entropy loss $\mathcal{L}_{\text{auxi}}$. The full objective for initializing the SA model is:

$$\mathcal{L} = \mathcal{L}_{\text{ratio}} + \mathcal{L}_{\text{auxi}}. \quad (12)$$

The classification token is enforced to be kept during the sparsification. It is discarded after the initialization. The

utility and budget models are initialized using $\mathcal{L}_{\text{utility}}$ and $\mathcal{L}_{\text{budget}}$, respectively.

Minimax optimization with auxiliary models. A minimax optimization strategy is applied to train the SA model. In this stage, the utility and budget models are *auxiliary*. They are iteratively updated along with the SA model. When updating the SA model, the full objective is:

$$\mathcal{L} = \mathcal{L}_{\text{ratio}} + \lambda_{\text{utility}}\mathcal{L}_{\text{utility}} - \lambda_{\text{budget}}\mathcal{L}_{\text{budget}}, \quad (13)$$

where we set $\lambda_{\text{utility}} = 0.5$ and $\lambda_{\text{budget}} = 0.5$ as default values. These coefficients are determined referring to their initial value scales without heavy tuning. Then the utility and budget models are updated using $\mathcal{L}_{\text{utility}}$ and $\mathcal{L}_{\text{budget}}$, respectively.

Training target models. After the minimax optimization, the SA model is frozen and the auxiliary models are discarded. To evaluate the efficacy of the SA model, new *target* utility and budget models are optimized on the transformed videos by using $\mathcal{L}_{\text{utility}}$ and $\mathcal{L}_{\text{budget}}$, respectively. Finally, the trained target models are adopted to evaluate their performances on the utility and budget tasks.

4. Experiments

4.1. Benchmarks

We choose two of the most popular large-scale action recognition datasets and manually annotate privacy labels for them as our benchmarks. **HMDB51** [20] is a collection of videos from movies and websites. It is composed of 6,849 videos from 51 actions and each category contains at least 101 videos. **UCF101** [31] consists of 13,320 videos taken from 101 actions. All actions can be grouped into five types, *i.e.*, body motion, human-human interactions, human-object interactions, playing musical instruments, and sports. To annotate privacy labels for these two datasets, we select five human-related attributes, *i.e.*, *face*, *skin color*, *gender*, *nudity*, and *familiar relationship*, referring to previous works [7, 39]. At least three annotators review each video and independently give their binary labels for each attribute according to whether the attribute is identifiable or not. Then the majority voting is adopted to decide each attribute label. The official training and testing splits for each dataset are used in our benchmarks.

4.2. Evaluation metrics

Top-1 accuracy is adopted to evaluate the performance of the utility task. The action of a video is determined by the averaged prediction of its 5 clips \times 3 crops [33]. Because the budget task is a multi-class binary classification problem, its performances are evaluated by classwise-mAP (cMAP) and classwise-F1 (F1) scores.

Method	HMDB51			UCF101		
	Top-1 (\uparrow)	F1 (\downarrow)	cMAP (\downarrow)	Top-1 (\uparrow)	F1 (\downarrow)	cMAP (\downarrow)
Raw data	51.44	0.673	75.58	84.20	0.684	76.62
Downsample-2 \times	40.80	0.601	71.35	72.79	0.620	71.49
Downsample-4 \times	31.32	0.594	69.79	56.07	0.615	69.85
Blackening [7]	38.27	0.649	74.06	69.41	0.660	75.37
StrongBlur [7]	40.91	0.655	74.33	73.94	0.672	75.58
WeakBlur [7]	47.24	0.663	75.11	77.31	0.678	76.03
Collective [41]	46.88	0.651	74.12	78.01	0.663	75.22
VITA [39]	48.11	0.638	73.89	78.49	0.657	75.36
SPAct [7]	48.56	0.642	73.78	78.40	0.651	75.29
Ours	50.73	0.613	72.48	82.55	0.634	73.79

Table 1. Comparison with SOTA methods on known actions. On each benchmark, our STPrivacy achieves the highest top-1 accuracy with the lowest F1 and cMAP scores (except the downsampling methods), *i.e.*, a significantly better trade-off between the utility and budget tasks.

Method	UCF101 \rightarrow HMDB51			HMDB51 \rightarrow UCF101		
	Top-1 (\uparrow)	F1 (\downarrow)	cMAP (\downarrow)	Top-1 (\uparrow)	F1 (\downarrow)	cMAP (\downarrow)
Raw data	51.44	0.673	75.58	84.20	0.684	76.62
Collective [41]	45.93	0.633	73.36	77.12	0.674	76.01
VITA [39]	46.78	0.621	73.47	77.48	0.669	76.02
SPAct [7]	47.81	0.618	72.56	78.13	0.661	75.98
Ours	49.56	0.595	71.25	81.04	0.645	74.60

Table 2. Comparison with SOTA methods on novel actions. In this challenging scenario, our STPrivacy outperforms all of them on two benchmarks.

4.3. Implementation details

Our framework is implemented based on ViT-S [10] using PyTorch. AdamW [23] with the weight decay 0.05 is adopted as the optimizer. The input video size is $16 \times 112 \times 112$ and the tubelet size is $2 \times 16 \times 16 \times 3$. The frame sampling rate on HMDB51 and UCF101 is 2 and 4, respectively. We linearly scale the learning rate *w.r.t.* the batch size with $0.001 \times \frac{\text{batch size}}{512}$, which decreases according to cosine annealing. All experiments are conducted on one NVIDIA TESLA V100 GPU and the batch size is 32. The numbers of training epochs for three stages are 80, 40, and 80, respectively. Please check our code for more details.

4.4. Comparison with state-of-the-art methods

We compare our framework with recent SOTA methods. For fair comparison, the same target models as ours are trained on the transformed videos by these methods. Two protocols, *i.e.*, evaluating on known and novel actions, are performed for comprehensive comparison. A higher top-1 accuracy with lower F1 and cMAP scores suggests a better method. Note that Downsample-2 \times and 4 \times simply reduce video resolutions, which indiscriminately decrease the utility and budget task performances. Therefore, we just report their results as references in the following tables and exclude them when comparing F1 and cMAP scores for convenient statement.

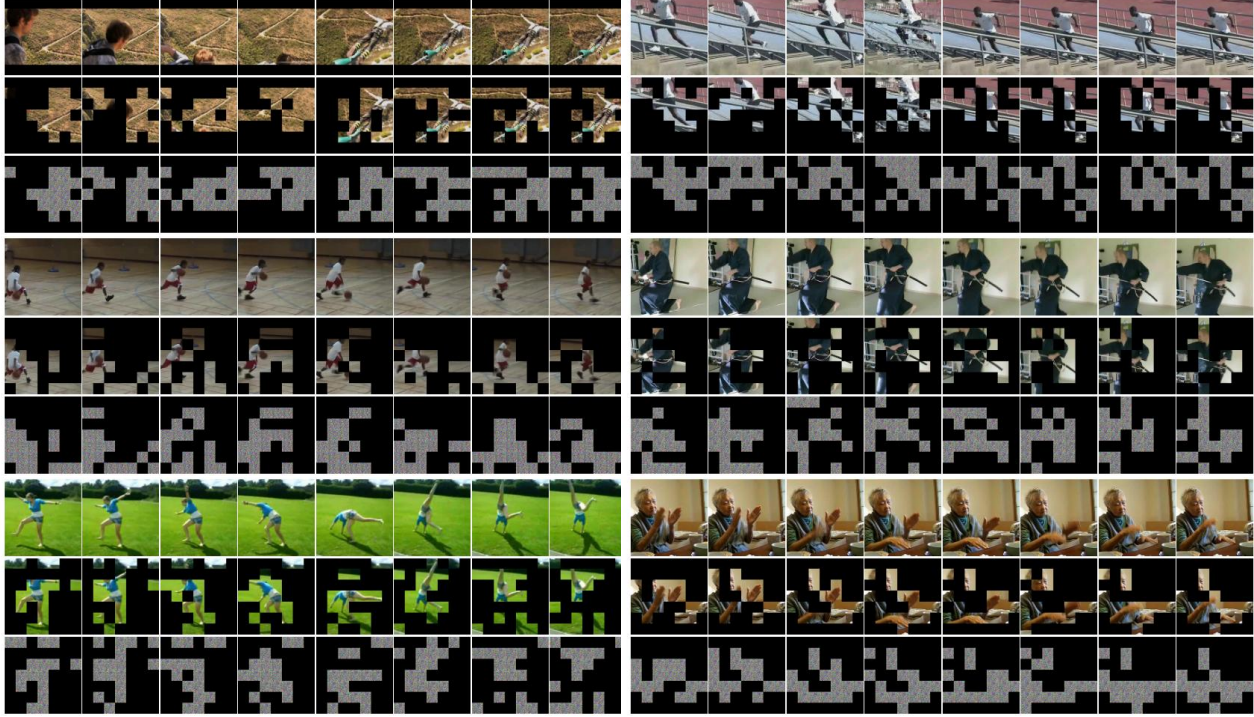


Figure 4. The visual efficacy illustration of our SA model for PPAR. Each group contains a raw input video, its final keeping decision, and anonymized remaining tubelets. In the left-right top-bottom order, the actions are *dive*, *climb stairs*, *dribble*, *draw sword*, *cartwheel*, and *clap*, sequentially. The perfect tubelet abandoning and the visually complete privacy removal in final outputs demonstrate our superiority.

Comparison on known actions. To evaluate our STPrivacy on the known action protocol, we train the SA model and the target models on the same benchmark. The results are reported in Table 1. Our framework has the best utility-budget performance trade-off on two benchmarks. On HMDB51, for example, compared with a typical method SPAct, our framework achieves a 2.17% higher top-1 accuracy with a 0.029 lower F1 score and a 1.3% lower cMAP score. On UCF101, compared with another SOTA method VITA, our results are also much better, *i.e.*, a 4.06% higher accuracy with a 0.023 lower F1 score and a 1.57% lower cMAP score. Overall, compared with the results on raw data, our framework has very small utility performance degradations but obtains large budget performance decreases.

Comparison on novel actions. To evaluate the efficacy of our STPrivacy on unseen actions, we train the SA model and the target models on different benchmarks. Namely the SA model does not see the evaluation actions during training. The results are reported in Table 2. Only learning-based methods have performance changes compared with the experiments on known actions. On UCF101→HMDB51, the utility performance drops due to the different action sets of training and evaluating. However, the F1 and cMAP scores also decrease apparently. It is because UCF101 covers a much wider range of life scenes than HMDB51. There-

fore, the SA model trained on UCF101 can better preserve the privacy information of HMDB51. This is also demonstrated by the consistently degraded performances of HMDB51→UCF101. In spite of these, our framework still achieves the best utility-budget trade-off.

4.5. Qualitative analysis

To qualitatively show the efficacy of our SA model, we visualize raw input videos, their final keeping decisions (projected to input tubelets), and anonymized remaining tubelets in Figure 4, where the black areas represent abandoned tubelets. Due to the high redundancy of adjacent frames, a half of frames from each video are shown.

Precisely abandoning action-irrelevant privacy tubelets.

Comparing the second row with the first in each group, we observe that the tubelets that contain private information but do not contribute to action dynamics are abandoned. In contrast, those tubelets involved in actions are kept. In *climb stairs*, for example, almost all head areas are abandoned to prevent the *face* information from leaking while the moving legs are kept to represent *climbing*. Other leg areas are also abandoned to preserve the *skin color* and *nudity* information. These demonstrate that our SA model can precisely distinguish privacy and action tubelets, realizing the automatic tubelets disentanglement, which is one of the reasons of our success. Note we do not pay attention to background tubelets that are irrelevant to either privacy or actions.

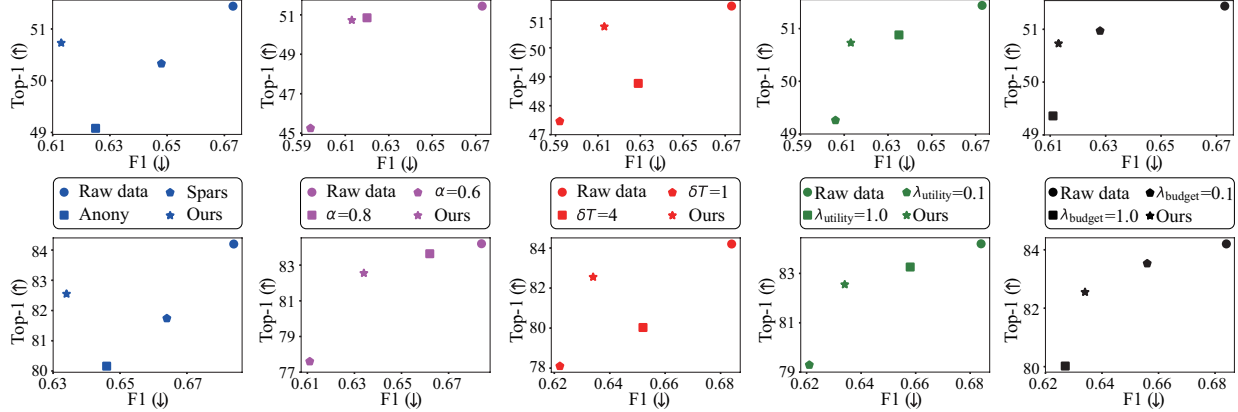


Figure 5. Ablation study results for the separate sparsification or anonymization (the 1st column), the tubelet keeping ratio (the 2nd column), the tubelet length (the 3rd column), λ_{utility} (the 4th column), and λ_{budget} (the last column) on HMDB51 (the 1st row) and UCF101 (the 2nd row). The method closest to the upper-left corner in each chart is the best.

Completely anonymizing action tubelets in visual space.

Comparing the third row with the second of each group, we observe that the remaining action tubelets are completely anonymized in visual space and humans can not identify any object silhouettes from them. This is much better than previous convolutional neural network-based learning methods, *e.g.*, ITNet [18] based VITA [39] and UNet [28] inspired SPAct [7], which intrinsically maintain object spatial information by stacking sliding convolutional kernels. In VITA [39], for example, humans can still easily identify silhouettes of salient objects from their anonymized frames. In contrast, token interaction-based ViTs [10] have inborn advantages of hiding geometric information of objects. This empowers our STPrivacy with the superiority of achieving the complete visual anonymization.

4.6. Ablation study

We conduct extensive ablation experiments to investigate the effect of our main components and key hyperparameters on two benchmarks. In each experiment, only the specified factor is changed and others remain the same as default (*ours*). All results are reported in Figure 5.

Sparsification effectively abandoning privacy tubelets.

To verify that our sparsification mechanism is able to abandon action-irrelevant privacy tubelets, we separately train the spars blocks of our SA model by feeding the input tubelets and corresponding final keeping decision, *i.e.*, O_{spars} in Figure 3, into the auxiliary models. The results of the downsampling methods in Table 1 suggest that the utility performance is much more easily decreased by indiscriminately transforming than the budget ones because the budget task does not require dynamic continuity. Therefore, compared with the raw data results, the smaller top-1 accuracy decrease ratio than those of the F1 and cMAP scores of the *spars* experiment demonstrates the effectiveness of our

sparsification.

Anonymization effectively maintaining action clues. To verify that our anonymization mechanism can maintain action clues when erasing private information in representation space, we train the SA model by setting all elements of three keeping decision matrices $\hat{\mathbf{I}}$ as 1, *i.e.*, enforcing all tubelets to be kept in each spars block. Compared with the raw data results, the much lower F1 and cMAP scores with the relatively high top-1 accuracy of the *anony* experiment demonstrate that our anonymization works as expected.

Tubelet keeping ratio balancing the utility and budget tasks.

We adjust the tubelet keeping ratio by setting different α in Equation 11. The performance changes on two benchmarks suggest that a larger α benefits action recognition but worsens the privacy leakage by encouraging the SA model to keep more tubelets and vice versa. Therefore, users can choose α according to their preferences between the utility and budget tasks, which contributes to our advantages over previous methods.

Tubelet length affecting the patch keeping flexibility.

We also adjust the tubelet temporal length δT , *i.e.*, the number of spatial patches. A tubelet with $\delta T = 1$ degenerates into a special case, only containing a single patch. Thus there are much more permutations for remaining tubelets, which makes the privacy removal easier. However, the single patch tubelet causes difficulties to representing temporal dynamics of actions. These are demonstrated by the decreased utility and budget performances of $\delta T = 1$ compared with *ours*. In contrast, another setting $\delta T = 4$ largely reduces the permutation flexibility of remaining tubelets, which clearly harms the trade-off between the utility and budget tasks.

Excellent robustness *w.r.t.* weighting coefficients.

To verify the robustness of our STPrivacy, we choose largely different values for λ_{utility} and λ_{budget} in Equation 13 for optimizing the SA model. A large value means the corresponding task is emphasized during transforming raw input

Method	Top-1 (↑)	F1 (↓)	cMAP (↓)
Raw data	73.13	0.714	78.51
Downsample-2×	54.53	0.259	54.33
Downsample-4×	41.67	0.244	47.17
StrongBlur [7]	56.77	0.331	63.61
WeakBlur [7]	64.22	0.369	64.19
Collective [41]	63.65	0.348	63.20
VITA [39]	66.43	0.314	61.09
SPAct [7]	67.12	0.326	62.78
Ours	71.37	0.280	59.30

Table 3. Comparison with SOTA methods for PPFR on Celeb-VHQ. Our framework works pretty well on the novel task.

videos and vice versa. The satisfactory performance fluctuations *w.r.t.* the wide range of hyper-parameter adjustments demonstrate our excellent robustness.

4.7. Generalizing to a novel task

To verify the generalization ability of our STPrivacy, we conduct experiments on a new task, *i.e.*, privacy-preserving facial expression recognition (PPFR). It is based on a facial video dataset **CelebVHQ** [45] consisting of 35,666 videos taken from 15,653 persons. Eight expressions, *i.e.*, *neutral*, *happy*, *sad*, *anger*, *fear*, *surprise*, *contempt*, and *disgust*, are annotated for all videos. Besides, various appearance attributes are provided. We select five of them as the privacy, *i.e.*, *young*, *pointy nose*, *male*, *rosy cheeks*, and *brown hair*. We randomly select 60% of all videos to construct the training set and leave the rest for the evaluation. The frame sampling rate is 2. All results are reported in Table 3. Note that the Blackening method fails here because it simply erases the detected persons. The comparison demonstrates that our framework can better separate the emotional dynamics from the appearance attributes. We also visualize the final keeping decision and anonymized remaining tubelets from the SA model for each raw video in Figure 6. In the second row of each group, we observe that only the facial areas closely related to expressing emotions, *e.g.*, a mouth, eyes, and cheeks, are kept and most of other parts, *e.g.*, hairs, are abandoned. In the third row, there are no visually identifiable details in the anonymized tubelets. In a word, the numerical and visualization results demonstrate the strong generalization ability of our framework.

4.8. Evaluating on frame-level privacy removal

Although our framework is specially designed for the video-level PPAR, we also conduct experiments to evaluate it on the frame-level privacy removal. PA-HMDB [39] is a video dataset with action labels and frame-level privacy attributes. In previous works [7, 39], it is only used for evaluating their target utility and budget models whose training is performed on HMDB51 and VISPR [24], respectively. However, this does not work here because VISPR is an image dataset and can not be transformed by our SA model. To enable the comparison, we randomly split PA-HMDB into

Method	Top-1 (↑)	F1 (↓)	cMAP (↓)
Raw data	51.23	0.572	71.12
Downsample-2×	40.38	0.519	67.81
Downsample-4×	31.24	0.511	67.14
Blackening [7]	38.09	0.557	70.02
StrongBlur [7]	40.64	0.560	70.31
WeakBlur [7]	46.89	0.567	70.74
Collective [41]	46.47	0.554	69.96
VITA [39]	47.78	0.549	69.45
SPAct [7]	48.33	0.543	69.44
Ours	50.61	0.523	68.76

Table 4. Comparison with SOTA methods for frame-level privacy removal on PA-HMDB. Our STPrivacy outperforms them easily.

a training set (60% videos) and a testing set (40% videos). HMDB51 is used to train the target utility model as before, while the frames from the training set are used to train the target budget model. Then the evaluation of the target models are performed on the testing set. Other methods also follow the same protocol. All results are reported in Table 4. The comparison suggests that our STPrivacy is still superior even on the frame-level privacy removal.

5. Conclusion

In this paper, we present a novel framework STPrivacy for video-level PPAR, which performs privacy preservation by adaptively sparsifying and anonymizing video tubelets in a unified manner. We also construct large-scale benchmarks for the community based on two of the most popular action recognition datasets. Additionally, we generalize our framework to a novel task named privacy-preserving facial expression recognition. Extensive experiments and detailed visualization analysis demonstrate the outstanding superiority of our STPrivacy over existing methods.

References

- [1] Anurag Arnab, Mostafa Dehghani, Georg Heigold, Chen Sun, Mario Lučić, and Cordelia Schmid. Vivit: A video vision transformer. In *Proceedings of the IEEE/CVF International Conference on Computer Vision*, pages 6836–6846, 2021. 2
- [2] Gedas Bertasius, Heng Wang, and Lorenzo Torresani. Is space-time attention all you need for video understanding? In *ICML*, volume 2, page 4, 2021. 2
- [3] Daniel J Butler, Justin Huang, Franziska Roesner, and Maya Cakmak. The privacy-utility tradeoff for remotely teleoperated robots. In *Proceedings of the tenth annual ACM/IEEE international conference on human-robot interaction*, pages 27–34, 2015. 2
- [4] Fabian Caba Heilbron, Victor Escorcia, Bernard Ghanem, and Juan Carlos Nibbles. Activitynet: A large-scale video benchmark for human activity understanding. In *Proceedings of the IEEE conference on computer vision and pattern recognition*, pages 961–970, 2015. 1
- [5] Edward Chou, Matthew Tan, Cherry Zou, Michelle Guo, Albert Haque, Arnold Milstein, and Li Fei-Fei. Privacy-

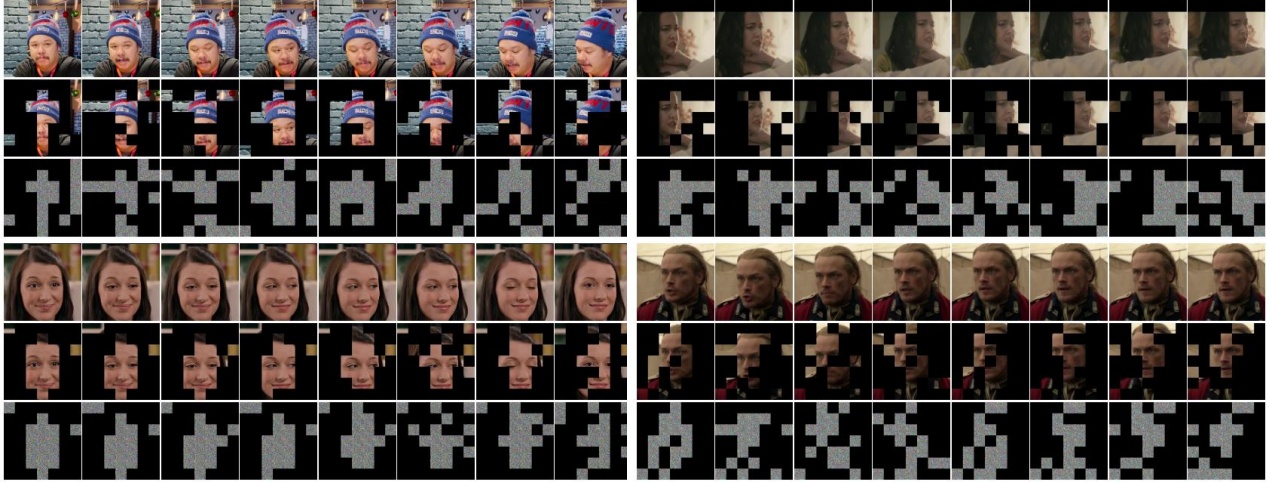


Figure 6. The visual efficacy of our SA model for PPFER. The sequential expressions in the left-right top-bottom order are *neutral*, *fear*, *happy*, and *sad*. The visualizations are highly in line with our expectations.

- preserving action recognition for smart hospitals using low-resolution depth images. *arXiv preprint arXiv:1811.09950*, 2018. 2
- [6] Ji Dai, Behrouz Saghaei, Jonathan Wu, Janusz Konrad, and Prakash Ishwar. Towards privacy-preserving recognition of human activities. In *2015 IEEE international conference on image processing (ICIP)*, pages 4238–4242. IEEE, 2015. 2
- [7] Ishan Rajendrakumar Dave, Chen Chen, and Mubarak Shah. Spact: Self-supervised privacy preservation for action recognition. In *Proceedings of the IEEE/CVF Conference on Computer Vision and Pattern Recognition*, pages 20164–20173, 2022. 2, 4, 5, 7, 8, 11
- [8] Jia Deng, Wei Dong, Richard Socher, Li-Jia Li, Kai Li, and Li Fei-Fei. Imagenet: A large-scale hierarchical image database. In *2009 IEEE conference on computer vision and pattern recognition*, pages 248–255. Ieee, 2009. 11
- [9] Jacob Devlin, Ming-Wei Chang, Kenton Lee, and Kristina Toutanova. Bert: Pre-training of deep bidirectional transformers for language understanding. *arXiv preprint arXiv:1810.04805*, 2018. 2
- [10] Alexey Dosovitskiy, Lucas Beyer, Alexander Kolesnikov, Dirk Weissenborn, Xiaohua Zhai, Thomas Unterthiner, Mostafa Dehghani, Matthias Minderer, Georg Heigold, Sylvain Gelly, et al. An image is worth 16x16 words: Transformers for image recognition at scale. *arXiv preprint arXiv:2010.11929*, 2020. 2, 3, 5, 7, 11
- [11] Christoph Feichtenhofer. X3d: Expanding architectures for efficient video recognition. In *CVPR*, 2020. 1
- [12] Christoph Feichtenhofer, Haoqi Fan, Yanghao Li, and Kaiming He. Masked autoencoders as spatiotemporal learners. *arXiv preprint arXiv:2205.09113*, 2022. 2
- [13] Christoph Feichtenhofer, Haoqi Fan, Jitendra Malik, and Kaiming He. Slowfast networks for video recognition. In *ICCV*, 2019. 1
- [14] Dan Hendrycks and Kevin Gimpel. Gaussian error linear units (gelus). *arXiv preprint arXiv:1606.08415*, 2016. 3
- [15] Ruibing Hou, Bingpeng Ma, Hong Chang, Xinqian Gu, Shiguang Shan, and Xilin Chen. Vrstc: Occlusion-free video person re-identification. In *Proceedings of the IEEE/CVF conference on computer vision and pattern recognition*, pages 7183–7192, 2019. 2
- [16] Ruibing Hou, Bingpeng Ma, Hong Chang, Xinqian Gu, Shiguang Shan, and Xilin Chen. Feature completion for occluded person re-identification. *IEEE Transactions on Pattern Analysis and Machine Intelligence*, 2021. 2
- [17] Eric Jang, Shixiang Gu, and Ben Poole. Categorical reparameterization with gumbel-softmax. *arXiv preprint arXiv:1611.01144*, 2016. 4
- [18] Justin Johnson, Alexandre Alahi, and Li Fei-Fei. Perceptual losses for real-time style transfer and super-resolution. In *European conference on computer vision*, pages 694–711. Springer, 2016. 7
- [19] Zhenglun Kong, Peiyan Dong, Xiaolong Ma, Xin Meng, Wei Niu, Mengshu Sun, Bin Ren, Minghai Qin, Hao Tang, and Yanzhi Wang. Spvit: Enabling faster vision transformers via soft token pruning. *arXiv preprint arXiv:2112.13890*, 2021. 2, 3, 4
- [20] Hildegard Kuehne, Hueihan Jhuang, Estíbaliz Garrote, Tomaso Poggio, and Thomas Serre. Hmdb: a large video database for human motion recognition. In *2011 International conference on computer vision*, pages 2556–2563. IEEE, 2011. 1, 2, 5
- [21] Tsung-Yi Lin, Michael Maire, Serge Belongie, James Hays, Pietro Perona, Deva Ramanan, Piotr Dollár, and C Lawrence Zitnick. Microsoft coco: Common objects in context. In *European conference on computer vision*, pages 740–755. Springer, 2014. 11
- [22] Jixin Liu and Leilei Zhang. Indoor privacy-preserving action recognition via partially coupled convolutional neural network. In *2020 International Conference on Artificial Intelligence and Computer Engineering (ICAICE)*, pages 292–295. IEEE, 2020. 2
- [23] Ilya Loshchilov and Frank Hutter. Decoupled weight decay regularization. *arXiv preprint arXiv:1711.05101*, 2017. 5
- [24] Tribhuvanesh Orekondy, Bernt Schiele, and Mario Fritz. Towards a visual privacy advisor: Understanding and predict-

- ing privacy risks in images. In *IEEE International Conference on Computer Vision (ICCV)*, 2017. 8
- [25] Bowen Pan, Rameswar Panda, Yifan Jiang, Zhangyang Wang, Rogerio Feris, and Aude Oliva. Ia-red²: Interpretability-aware redundancy reduction for vision transformers. *Advances in Neural Information Processing Systems*, 34:24898–24911, 2021. 2, 3
- [26] Yongming Rao, Wenliang Zhao, Benlin Liu, Jiwen Lu, Jie Zhou, and Cho-Jui Hsieh. Dynamicvit: Efficient vision transformers with dynamic token sparsification. *Advances in neural information processing systems*, 34:13937–13949, 2021. 2, 3, 4, 11
- [27] Zhongzheng Ren, Yong Jae Lee, and Michael S Ryoo. Learning to anonymize faces for privacy preserving action detection. In *Proceedings of the european conference on computer vision (ECCV)*, pages 620–636, 2018. 2
- [28] Olaf Ronneberger, Philipp Fischer, and Thomas Brox. U-net: Convolutional networks for biomedical image segmentation. In *International Conference on Medical image computing and computer-assisted intervention*, pages 234–241. Springer, 2015. 7
- [29] Michael S Ryoo, Brandon Rothrock, Charles Fleming, and Hyun Jong Yang. Privacy-preserving human activity recognition from extreme low resolution. In *Thirty-First AAAI Conference on Artificial Intelligence*, 2017. 2
- [30] Dian Shao, Yue Zhao, Bo Dai, and Dahua Lin. Finegym: A hierarchical video dataset for fine-grained action understanding. In *Proceedings of the IEEE/CVF conference on computer vision and pattern recognition*, pages 2616–2625, 2020. 1
- [31] Khurram Soomro, Amir Roshan Zamir, and Mubarak Shah. Ucf101: A dataset of 101 human actions classes from videos in the wild. *arXiv preprint arXiv:1212.0402*, 2012. 1, 2, 5
- [32] Vinkle Srivastav, Afshin Gangi, and Nicolas Padoy. Human pose estimation on privacy-preserving low-resolution depth images. In *International Conference on Medical Image Computing and Computer-Assisted Intervention*, pages 583–591. Springer, 2019. 2
- [33] Zhan Tong, Yibing Song, Jue Wang, and Limin Wang. Videomae: Masked autoencoders are data-efficient learners for self-supervised video pre-training. *arXiv preprint arXiv:2203.12602*, 2022. 2, 5
- [34] Hugo Touvron, Matthieu Cord, Matthijs Douze, Francisco Massa, Alexandre Sablayrolles, and Hervé Jégou. Training data-efficient image transformers & distillation through attention. *arXiv preprint arXiv:2012.12877*, 2020. 11
- [35] Du Tran, Heng Wang, Lorenzo Torresani, Jamie Ray, Yann LeCun, and Manohar Paluri. A closer look at spatiotemporal convolutions for action recognition. In *Proceedings of the IEEE conference on Computer Vision and Pattern Recognition*, pages 6450–6459, 2018. 1
- [36] Ashish Vaswani, Noam Shazeer, Niki Parmar, Jakob Uszkoreit, Llion Jones, Aidan N Gomez, Łukasz Kaiser, and Illia Polosukhin. Attention is all you need. In *NeurIPS*, pages 5998–6008, 2017. 2, 4
- [37] Limin Wang, Yuanjun Xiong, Zhe Wang, Yu Qiao, Dahua Lin, Xiaoou Tang, and Luc Van Gool. Temporal segment networks for action recognition in videos. *IEEE TPAMI*, 2019. 1
- [38] Yingquan Wang, Pingping Zhang, Shang Gao, Xia Geng, Hu Lu, and Dong Wang. Pyramid spatial-temporal aggregation for video-based person re-identification. In *Proceedings of the IEEE/CVF International Conference on Computer Vision (ICCV)*, pages 12026–12035, October 2021. 2
- [39] Zhenyu Wu, Haotao Wang, Zhaowen Wang, Hailin Jin, and Zhangyang Wang. Privacy-preserving deep action recognition: An adversarial learning framework and a new dataset. *IEEE Transactions on Pattern Analysis and Machine Intelligence*, 2020. 2, 4, 5, 7, 8, 11
- [40] Zhenyu Wu, Zhangyang Wang, Zhaowen Wang, and Hailin Jin. Towards privacy-preserving visual recognition via adversarial training: A pilot study. In *Proceedings of the European Conference on Computer Vision (ECCV)*, pages 606–624, 2018. 2, 4
- [41] Dalin Zhang, Lina Yao, Kaixuan Chen, Guodong Long, and Sen Wang. Collective protection: Preventing sensitive inferences via integrative transformation. In *2019 IEEE International Conference on Data Mining (ICDM)*, pages 1498–1503. IEEE, 2019. 5, 8, 11
- [42] Zhixiang Zhang, Thomas Cilloni, Charles Walter, and Charles Fleming. Multi-scale, class-generic, privacy-preserving video. *Electronics*, 10(10):1172, 2021. 2
- [43] Zhizheng Zhang, Cuiling Lan, Wenjun Zeng, and Zhibo Chen. Multi-granularity reference-aided attentive feature aggregation for video-based person re-identification. In *Proceedings of the IEEE/CVF conference on computer vision and pattern recognition*, pages 10407–10416, 2020. 2
- [44] Haoyi Zhou, Shanghang Zhang, Jieqi Peng, Shuai Zhang, Jianxin Li, Hui Xiong, and Wancai Zhang. Informer: Beyond efficient transformer for long sequence time-series forecasting. *arXiv preprint arXiv:2012.07436*, 2020. 2
- [45] Hao Zhu, Wayne Wu, Wentao Zhu, Liming Jiang, Siwei Tang, Li Zhang, Ziwei Liu, and Chen Change Loy. CelebV-HQ: A large-scale video facial attributes dataset. In *ECCV*, 2022. 2, 8

STPrivacy: Spatio-Temporal Tubelet Sparsification and Anonymization for Privacy-preserving Action Recognition

APPENDIX

1. Details of current SOTA methods

Downsample-2 \times and 4 \times represent downsampling input video resolutions with different rates. Blackening refers to detecting person bounding boxes from each video frame by using MS-COCO [21] pre-trained YOLOv5x* and filling zero values in the detected regions. StrongBlur and WeakBlur are applying different Gaussian blur filters within the detected bounding boxes. Collective [41] is extended from a non-visual privacy preservation method proposed for wearable devices. Please refer to [7] for more details. VITA [39] and SPAct [7] are implemented based on their source codes and papers. All these methods perform the frame-level (spatial) privacy preservation and ignore action continuity. In contrast, our STPrivacy is proposed to perform the video-level (spatio-temporal) privacy preservation by employing both the tubelet sparsification and anonymization mechanisms in a unified manner, which emphasizes action dynamics for the utility task. Our framework is implemented based on ViT-S [10, 26, 34] pre-trained on ImageNet [8].

2. All ablation experiment results

In Section 4.6, we show top-1 accuracy and F1 score of each ablation experiment in a scatter chart, which can help to easily compare the utility-budget performance trade-offs. Due to the space limitation, we report all ablation experiment results in Table 5.

Method	HMDB51			UCF101		
	Top-1 (\uparrow)	F1 (\downarrow)	cMAP (\downarrow)	Top-1 (\uparrow)	F1 (\downarrow)	cMAP (\downarrow)
Raw data	51.44	0.673	75.58	84.20	0.684	76.62
Spars	50.33	0.648	74.18	81.74	0.664	75.98
Anony	49.08	0.625	73.84	80.16	0.646	75.35
$\alpha = 0.6$	45.25	0.594	71.14	77.60	0.611	72.38
$\alpha = 0.8$	50.85	0.620	72.95	83.64	0.662	74.07
$\delta T = 1$	47.46	0.592	71.11	78.10	0.622	71.97
$\delta T = 4$	48.77	0.629	73.71	80.03	0.652	75.15
$\lambda_{\text{utility}} = 0.1$	49.26	0.606	71.28	79.29	0.621	72.13
$\lambda_{\text{utility}} = 1.0$	50.88	0.635	73.44	83.26	0.658	75.18
$\lambda_{\text{budget}} = 0.1$	50.97	0.628	73.72	83.53	0.656	75.44
$\lambda_{\text{budget}} = 1.0$	49.36	0.611	71.78	80.02	0.627	72.91
Ours	50.73	0.613	72.48	82.55	0.634	73.79

Table 5. All ablation study results for the main components and key hyper-parameters of our STPrivacy.

3. More visualization results

Due to the space limitation, we only show the visual efficacy of our SA model for PPAR on a couple of actions in Section 4.5. Here we provide more visualization results in Figure 7, 8, and 9. From them, we observe that our sparsification mechanism can perfectly abandon action-irrelevant privacy tubelets and then our anonymization mechanism is able to completely remove visual clues of objects from the remaining tubelets. These are the reasons why our STPrivacy is effective and superior over current SOTA methods.

*<https://github.com/ultralytics/yolov5>



Figure 7. The visual efficacy illustration of our SA model for PPAR. Each group contains a raw input video, its final keeping decision, and anonymized remaining tubelets. In the top-bottom order, the actions are *push*, *pour*, *golf*, and *pullup*, sequentially.

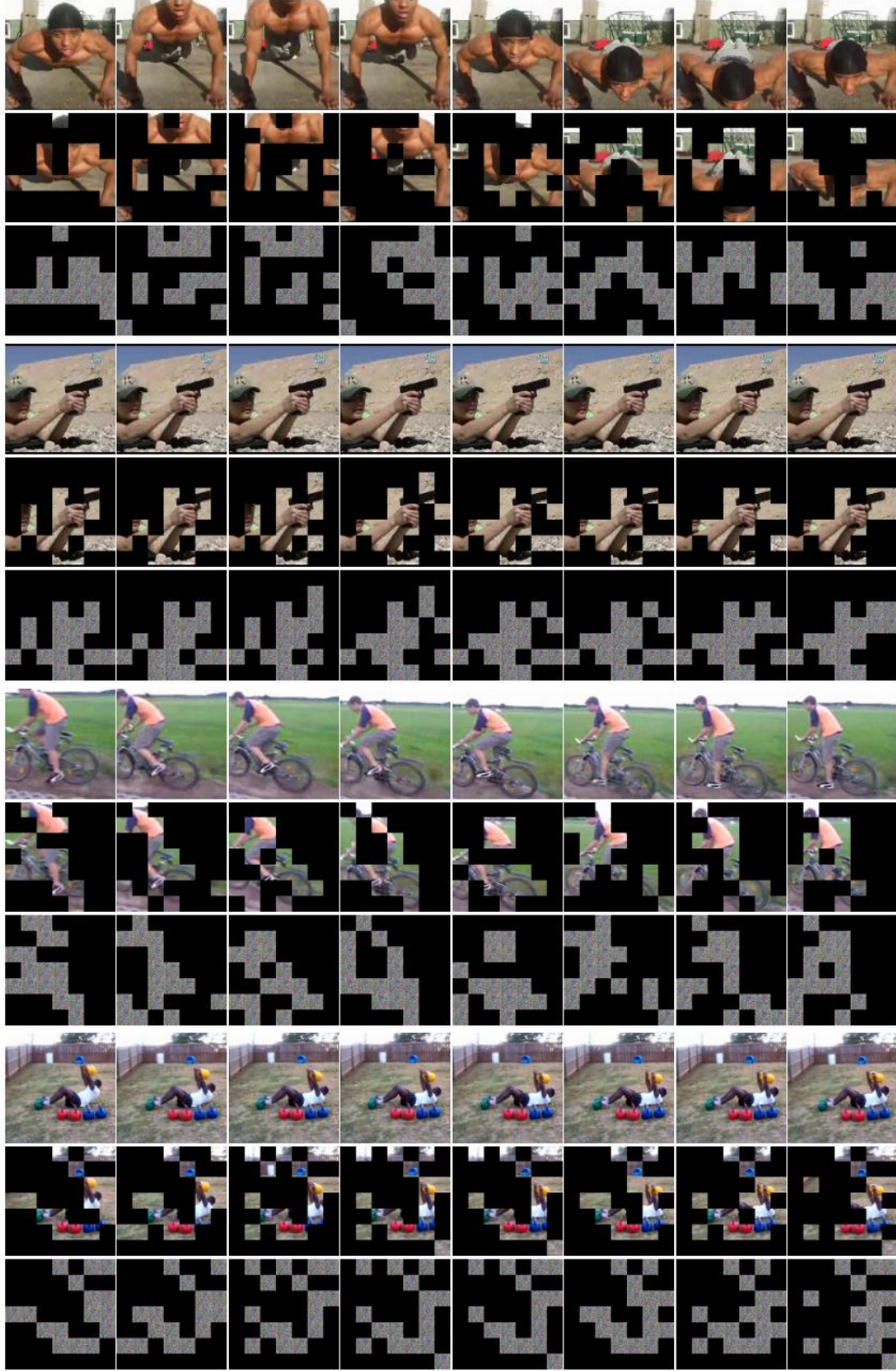


Figure 8. The visual efficacy illustration of our SA model for PPAR. Each group contains a raw input video, its final keeping decision, and anonymized remaining tubelets. In the top-bottom order, the actions are *pushup*, *shoot gun*, *ride bike*, and *situp*, sequentially.

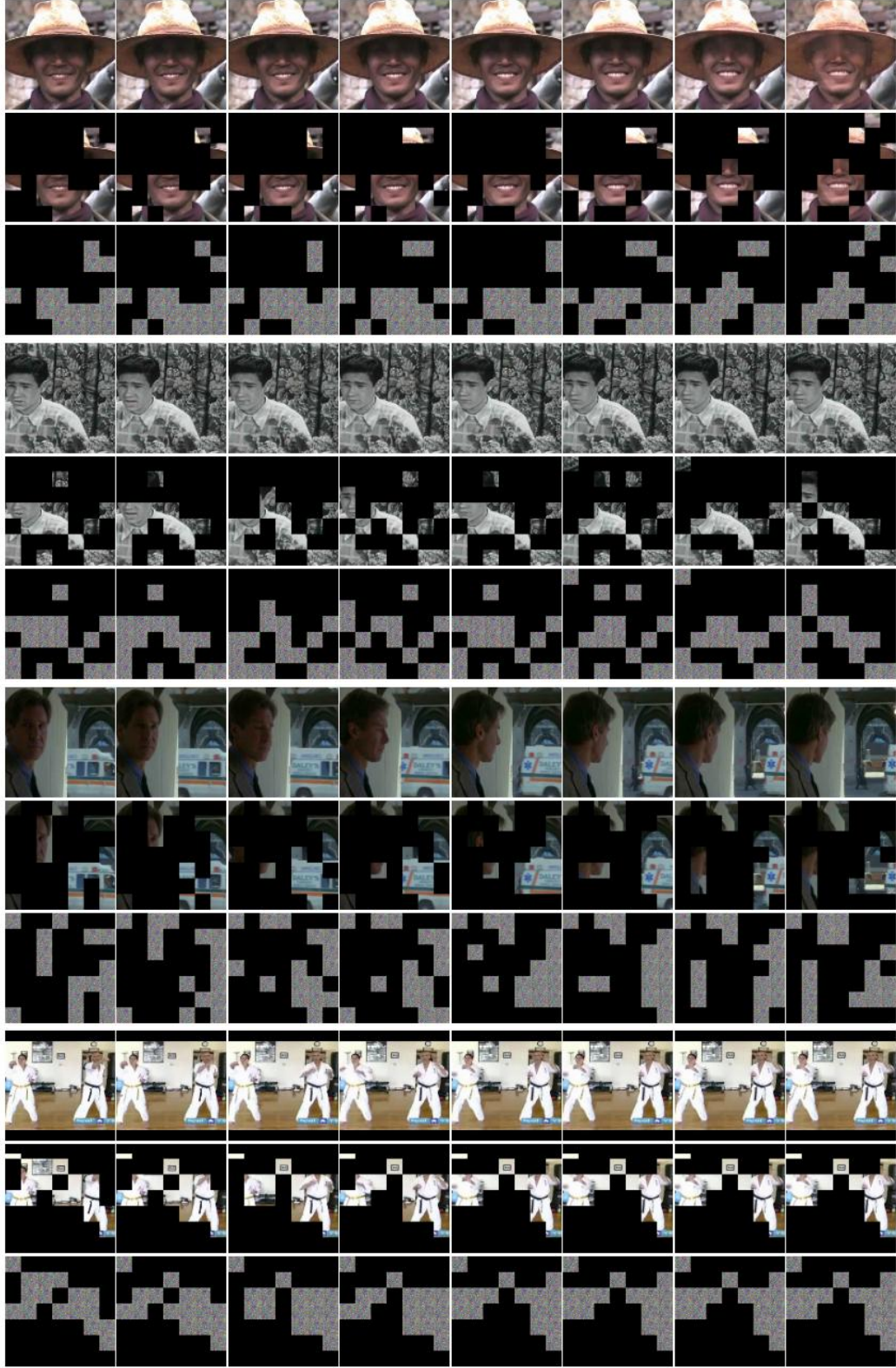


Figure 9. The visual efficacy illustration of our SA model for PPAR. Each group contains a raw input video, its final keeping decision, and anonymized remaining tubelets. In the top-bottom order, the actions are *smile*, *talk*, *turn*, and *punch*, sequentially.